

Evolution of electronic and ionic structure of Mg-clusters with the growth cluster size

Andrey Lyalin, Ilia A. Solov'yov,^y Andrey V. Solov'yov,^z and Walter Greiner

Institut für Theoretische Physik der Universität Frankfurt am Main,

Robert-Mayer-Str. 8-10, D-60054 Frankfurt am Main, Germany

The optimized structure and electronic properties of neutral and singly charged magnesium clusters have been investigated using ab initio theoretical methods based on density-functional theory and systematic post-Hartree-Fock many-body perturbation theory accounting for all electrons in the system. We have systematically calculated the optimized geometries of neutral and singly charged magnesium clusters consisting of up to 21 atoms, electronic shell closures, binding energies per atom, ionization potentials and the gap between the highest occupied and the lowest unoccupied molecular orbitals. We have investigated the transition to the hcp structure and metallic evolution of the magnesium clusters, as well as the stability of linear chains and rings of magnesium atoms. The results obtained are compared with the available experimental data and the results of other theoretical works.

I. INTRODUCTION

Metal clusters have been recognized as new physical objects with their own properties almost two decades ago. This became clear after such experimental successes as the discovery of electronic shell structure in metal clusters [1], observation of plasmon resonances [2, 3, 4], formation of singly and doubly charged negative cluster ions [5] and many more.

^xPermanent address: Institute of Physics, St. Petersburg State University, 198504 St. Petersburg, Petrodvorez, Russia; Email address: lyalin@th.physik.uni-frankfurt.de

^yPermanent address: A. F. Ioffe Physical Technical Institute, 194021 St. Petersburg, Russia; Email address: ilia@th.physik.uni-frankfurt.de

^zPermanent address: A. F. Ioffe Physical Technical Institute, 194021 St. Petersburg, Russia; Email address: solovyov@th.physik.uni-frankfurt.de

Comprehensive survey of the field can be found in review papers and books; see, e.g., [6, 7, 8, 9, 10, 11, 12, 13, 14].

The electronic shell structure of metal clusters has been discovered in [1] by the observation of the strong pics in the mass spectra of sodium clusters. The enhanced stability of some clusters, the so-called magic clusters, was explained by the closure of shells of delocalized electrons. A simple physical model describing electronic shell structure of metal clusters has been developed within the jellium approximation (see, e.g., [6]) by analogy with the shell model of atomic nuclei (see, e.g., [15]). The jellium model is very successful for the simple alkali metals (Na, K), for which one electron per atom is delocalized [16, 17, 18]. The jellium model electronic shell closures for alkali metal clusters define themagic numbers $N = 8, 20, 34, 40, 58, 92$ that are in a good agreement with experiment. Note that the jellium model can be generalized by accounting for the collective ion background vibration dynamics [19, 20] and be used as a very appropriate framework for the investigating collision processes involving atomic clusters [21].

Clusters of divalent metals are expected to differ from the jellium model predictions at least at small cluster sizes. In this case, bonding between atoms is expected to have some features of the van der Waals type of bonding, because the electronic shells in the divalent atoms are filled. Thus, clusters of divalent metals are very appropriate for studying non-metal to metal transition, testing different theoretical methodologies and conceptual developments of atomic cluster physics. However, relatively little work was done so far on the exploration of the alkali-earth metal clusters in comparison with that for the alkali metal clusters; see, e.g., [6, 22] and references therein.

Previous theoretical studies of the magnesium cluster properties have been performed using pseudopotential approximation for the treatment of inner electrons in a cluster and the density-functional theory for the description of outer shell electrons. The electronic properties, geometry and stability of small Mg metal clusters with the number of atoms $N \leq 7$ have been investigated in [23, 24] using the pseudopotential local-spin-density approximation. The geometrical structure and bonding nature of Mg_N clusters with N up to 13 have been studied in [25] using the density-functional molecular-dynamics method. The size evolution of bonding in magnesium clusters Mg_N with $N = 8-13, 16, 20$ have been studied in [26] using the local-density approximation that accounts for gradient corrections. Structural and electronic properties of small magnesium clusters ($N \leq 13$) were studied in

[27] using a first-principles simulation method in conjunction with the density-functional theory and the generalized gradient correction approximation for the exchange-correlation functional. It was shown [27] that the metallization in magnesium clusters has a slow and nonmonotonic evolution, although, also jellium-type magic clusters were observed [25, 26]. In order to extend such calculations to larger systems, symmetry restricted methods have been developed. The spherically-averaged-pseudo-potential scheme with the local and non-local pseudopotentials has been used for the investigation of the electronic structure and shell closures of spherical Mg_N clusters up to $N = 46$ [28].

Recently, new experimental data for Mg clusters have been obtained, indicating the most intensive pics in the mass spectra at $N = 5, 10, 15, 18, 20, 25, 28, 30, 35, 40, 47, 56, 59, 62$, and 69 [29]. These numbers deviate from the sequence of magic numbers which were obtained for simple alkali metal clusters, and cannot be reproduced within simple jellium models. This fact was interpreted in [29, 30] within the spherical shell model by diving of the high angular momentum states down through the states with lower l .

In the present work we investigate the optimized ionic structure and the electronic properties of neutral and singly charged magnesium clusters within the size range $N = 21$. We calculate binding energies per atom, ionization potentials and energy gaps between the highest occupied and the lowest unoccupied molecular orbitals. Our calculations are based on ab initio theoretical methods invoking the density-functional theory and systematic post-Hartree-Fock many-body theory accounting for all electrons in the system. The results obtained are compared with the available experimental data and the results of other theoretical works.

The atomic system of units, $je = m_e = h = 1$, has been used throughout the paper, unless other units are indicated.

II. THEORETICAL METHODS

Our calculations have been performed with the use of the Gaussian 98 software package [31]. We have utilized the 6-311G(d) basis set of primitive Gaussian functions to expand the cluster orbitals [31, 32].

The cluster geometries have been determined by finding local minima on the multidimensional potential energy surface for a cluster. We have taken into account all electrons

available in the system, when computing the potential energy surface. With increasing cluster size, such calculations become computer time demanding. In this work, we limit the calculations by the cluster size $N = 21$.

The key point of calculations is fixing the starting geometry of the cluster, which could converge during the calculation to a local or the global minimum. There is no unique way for achieving this goal with Gaussian 98 [32]. In our calculations, we have created the starting geometries empirically, often assuming certain cluster symmetries. Note, that during the optimization process the geometry of the cluster as well as its initial symmetry sometimes change dramatically. All the characteristics of clusters, which we have calculated and present in next section, are obtained for the clusters with optimized geometry.

In this work we concentrate on the systematic exploration of the properties of magnesium clusters using the density-functional theory based on the hybrid Becke-type three-parameter exchange functional [33] paired with the gradient-corrected Lee, Yang and Parr correlation functional (B3LYP) [34, 35], as well as the gradient-corrected Perdew-Wang 91 correlation functional (B3PW91) [36, 37]. The important feature of the density-functional method consists in the fact that it takes into account many-electron correlations via the phenomenological exchange-correlation potential. However, so far, there has not been found the unique potential, universally applicable for different systems and conditions. As a result there are many different parameterizations for the exchange-correlation potential valid for special cases.

Alternatively, we use a direct ab initio method for the description of electronic properties of metal clusters, which is based on the consistent post-Hartree-Fock many-body theory [38]. In the present work, we apply the Muller-Plesset perturbation theory of the fourth order (MP4). Based on the fundamental physical principles being free from any phenomenological parameters, this model can be refined by extending the quality of the approximations, while the physical meaning of the effects included is clearly demonstrated. Thus, often such an approach predicts more accurate and reliable characteristics of metal clusters than the density-functional theory.

In the present work we use both different theoretical schemes for calculations taking advantage of the clear physical meaning and reliability of the post-Hartree-Fock perturbation theory and the numerical efficiency of the density-functional methods.

III. NUMERICAL RESULTS AND DISCUSSION

A. Geometry optimization of Mg_N and Mg_N^+ clusters

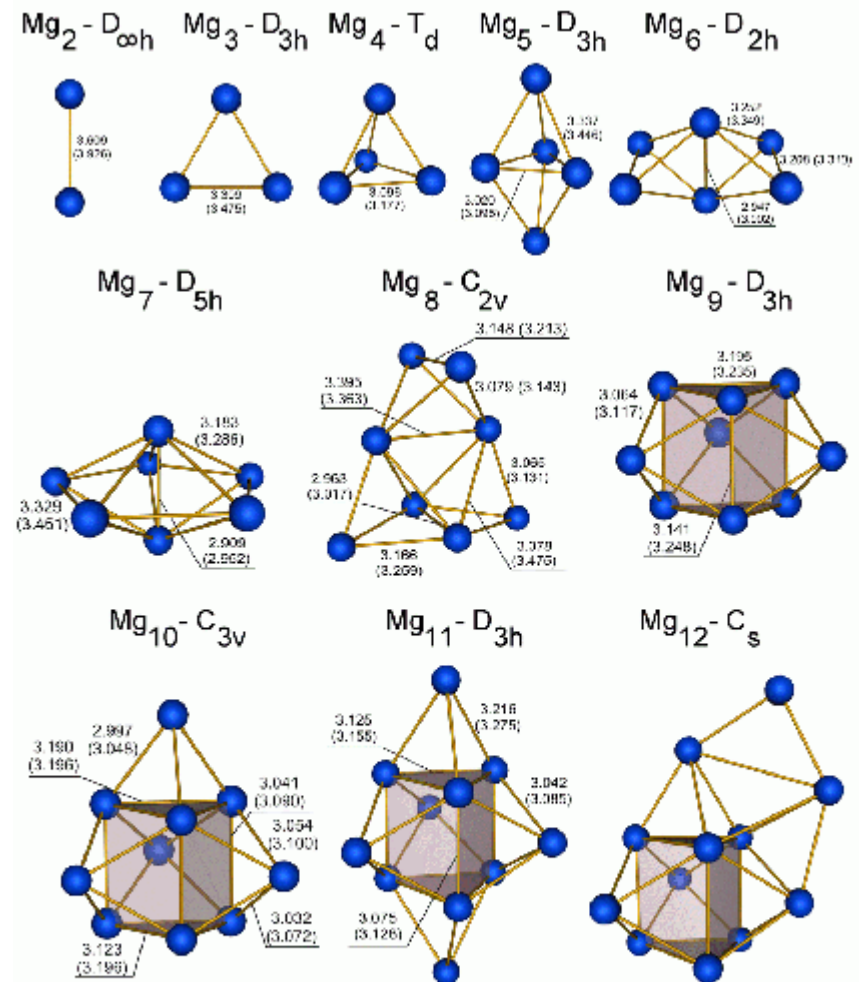
The optimization of the cluster geometries has been performed with the use of the B3PW91 and B3LYP methods. For small magnesium clusters with number of atoms $N = 11$, we have also used the ab initio MP4 method in addition to density-functional calculations. With the growth cluster size the ab initio MP4 calculations become more and more computer time demanding, therefore we have not performed such calculations for magnesium clusters with the number of atoms $N = 12$. The detail comparison of the results obtained by the density-functional and ab initio perturbation theory methods as well as their comparison with the results of other works is given below, see section IIIB. This comparison allows us to conclude that for magnesium clusters the B3PW91 method is more reliable and accurate in comparison with the B3LYP one.

The results of the cluster geometry optimization for neutral and singly charged magnesium clusters consisting of up to 21 atoms are shown in figures 1 and 2 respectively.

Magnesium clusters possess various isomers for those number grows dramatically with increasing cluster size. In figures 1 and 2, we present only the lowest energy configurations optimized by the B3PW91 method. The interatomic distances are given in angstroms. The values in brackets correspond to the interatomic distances obtained by the B3LYP method.

Figure 1 shows that the neutral magnesium clusters form the compact structures, maximizing the coordination number. The Mg_2 dimer is weakly bound possessing the binding energy per atom 0.039 eV/atom and the bond length 3.609 Å, which is in a good agreement with the experimental results of Ref. [39], where the values 0.025 eV/atom for the binding energy and 3.89 Å and for the bond length have been reported. The lowest energy state for Mg_3 is the equilateral triangle, and for Mg_4 is a regular tetrahedron. As we discuss below, the Mg_4 cluster is relatively more stable and compact, as compared to the neighbouring clusters. The Mg_5 cluster has a structure of slightly elongated triangular bipyramid, while Mg_6 is a bipyramid with rectangular basis and Mg_7 is a pentagonal bipyramid. These geometrical structures are in a good agreement with the results of Ref. [24].

It is worth to note that the optimized geometry structures for small neutral magnesium clusters differ significantly from those obtained for sodium clusters (see, e.g., [22, 40, 41]



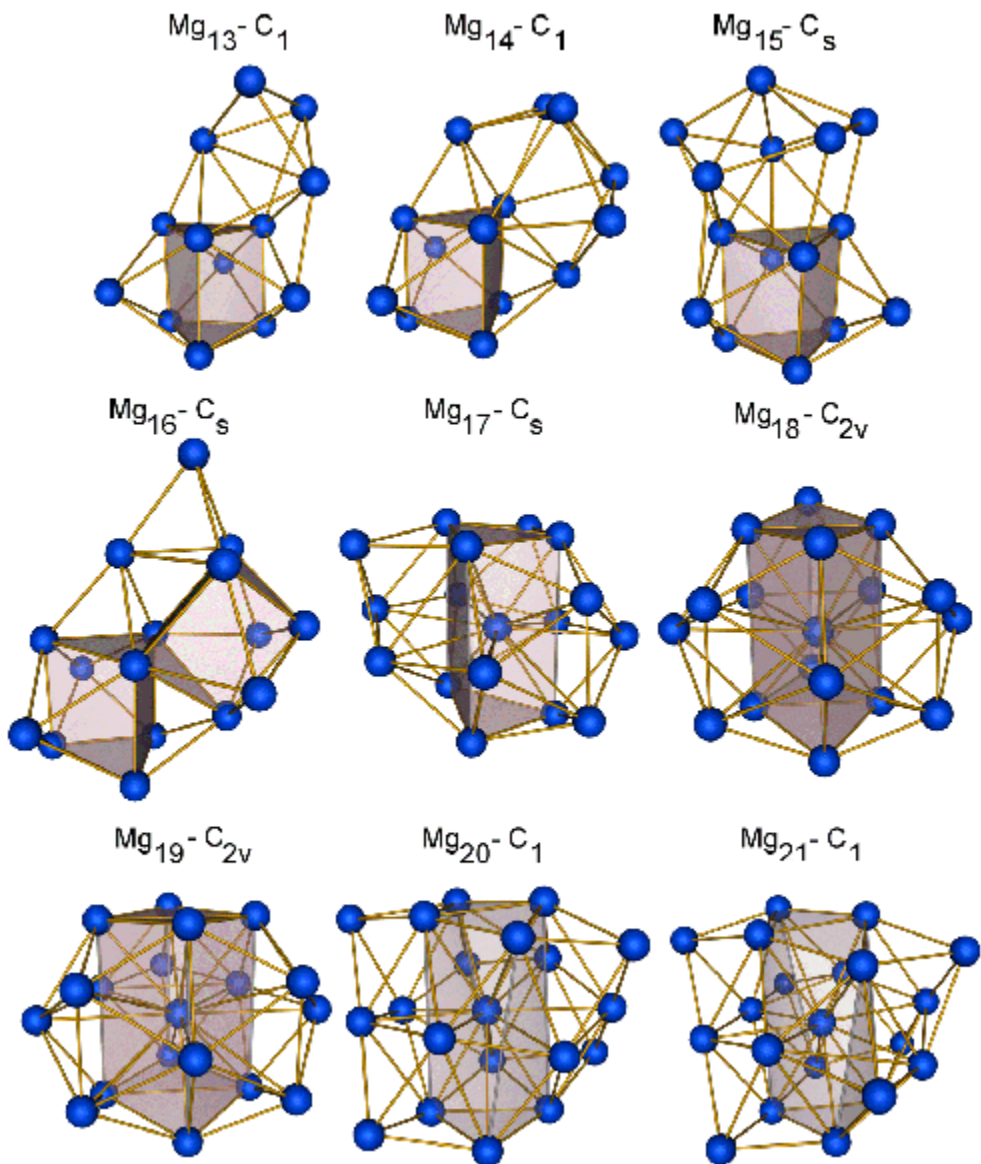
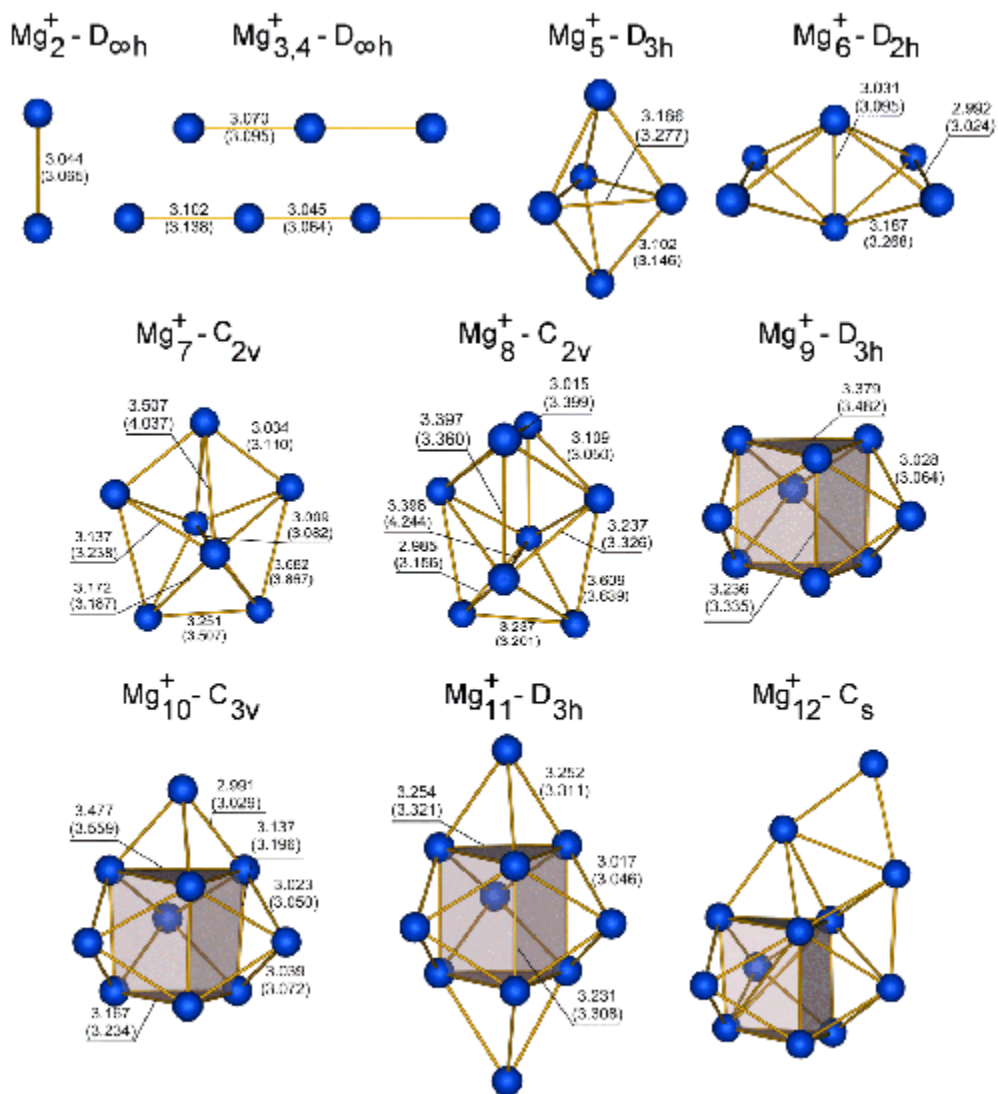


FIG . 1: Optimized geometries of the neutral magnesium clusters Mg_2 – Mg_{21} calculated in the B3PW91 approximation. The interatomic distances are given in angstroms. The values in brackets correspond to the B3LYP results. The label above each cluster indicates the point symmetry group of the cluster.



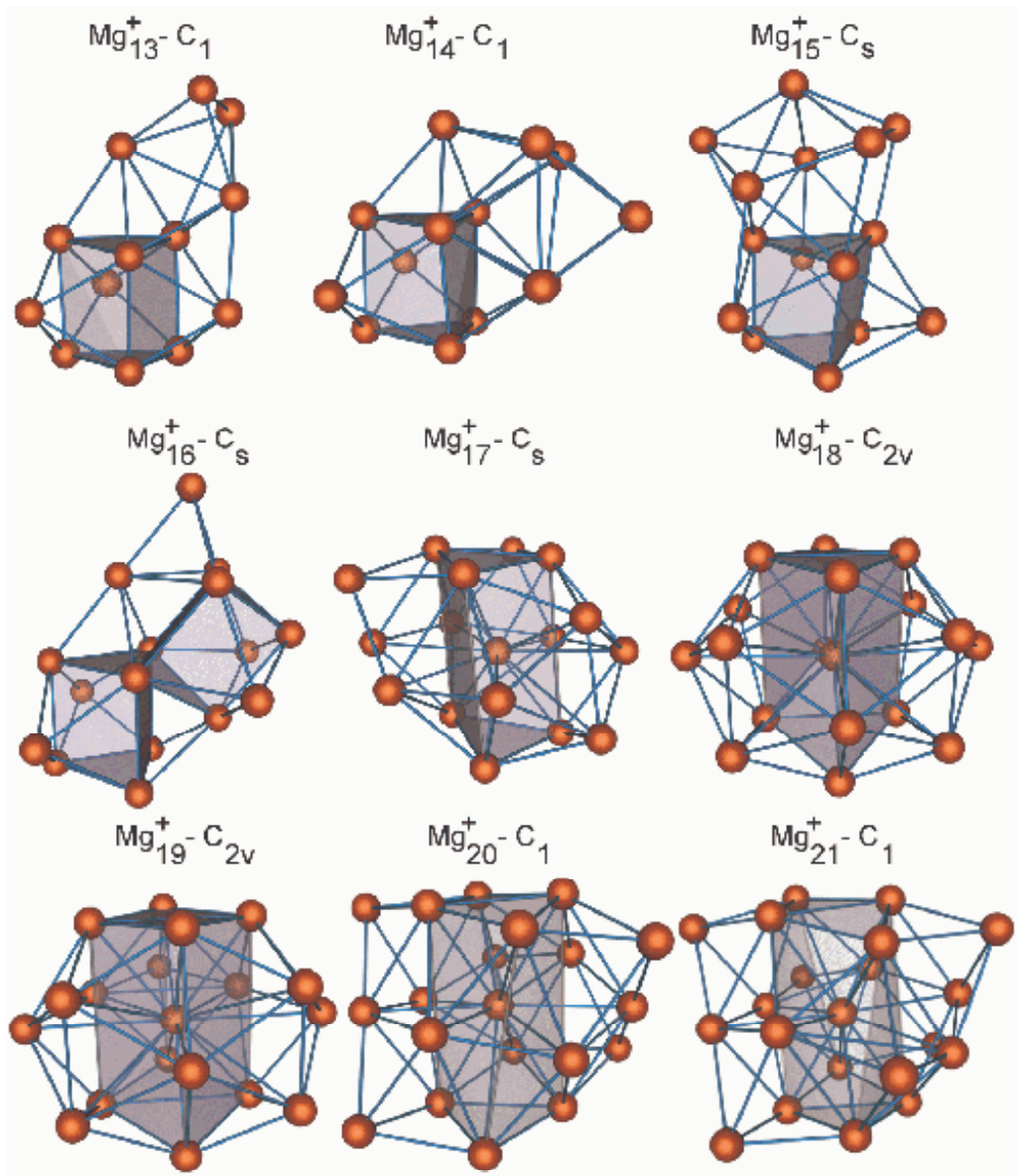


FIG. 2: The same as in Fig.1 but for singly-charged magnesium clusters $Mg_2^+ - Mg_{21}^+$.

and references therein). Thus, the optimized sodium clusters with $N = 6$ have the plane structure. For $N \geq 6$, both plane and spatial isomers with very close total energies exist. The planar behavior of small sodium clusters has been explained as a result of the successive filling of the orbitals 1 and 1 symmetry by delocalized valence electrons [40], which is fully consistent with the deformed jellium model calculations [18]. Contrary to the small sodium clusters, the magnesium clusters are tridimensional already at $N = 4$, forming the structures nearly the same as the van der Waals bonded clusters.

Starting from Mg_9 a new element appears in the magnesium cluster structures. This is the six atom trigonal prism core, which is marked out in figure 1. The formation of the trigonal prism plays the important role in the magnesium cluster growth process. Adding an atom to one of the triangular faces of the trigonal prism of the Mg_9 cluster results in the Mg_{10} structure, while adding an atom to the remaining triangular face of the prism within the Mg_{10} cluster leads to the structure of Mg_{11} , as shown in figure 1.

Further growth of the magnesium clusters for $12 \leq N \leq 16$ leads to the formation of the low symmetry ground state cluster. In spite of their low symmetry, all these clusters have the trigonal prism core. Some structural rearrangement occurs for the Mg_{16} cluster, which results in the structure with two connected triangular prisms.

Starting from Mg_{17} another motif based on the three-layered trigonal prism dominates the cluster growth. This prism is the basic element of the hexagonal closest-packing (hcp) lattice, as one can see in figure 3, where the primitive cell for the magnesium hcp lattice is presented. Thus, $N = 17$ is the turning-point in the formation of the hcp lattice for magnesium.

Vectors a , b and c in figure 3 show the primitive cell axes of the hcp lattice. For bulk magnesium $a = b = 3.21 \text{ \AA}$ and $c = 5.21 \text{ \AA}$ [42]. The fundamental characteristic for the hexagonal closest-packing of spheres is the value of ratio c/a , which is equal to $\sqrt[3]{8/3} = 1.633$ for ideal hcp lattice. The bulk magnesium with $c/a = 1.62$ is very close to ideal hcp structure [43].

Table I presents the averaged values of the primitive axes h_{ci} and h_{ai} for trigonal prisms marked out in figure 1 for magnesium clusters with the number of atoms $N \leq 17$. Table I demonstrates that the values h_{ci} and h_{ai} and their ratio for magnesium clusters with $N \leq 17$ are very close to the respective values for bulk magnesium.

Figure 2 shows the optimized geometries of singly-charged cationic magnesium clusters.

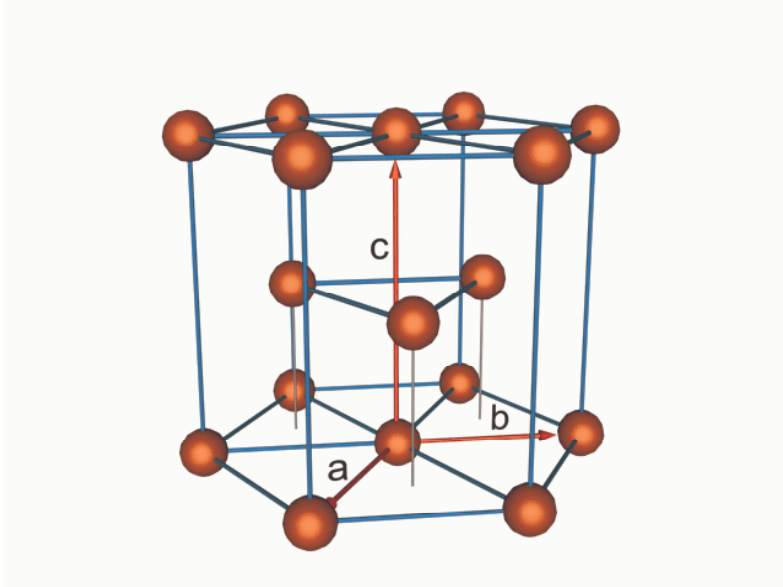


FIG. 3: Primitive cell for magnesium hcp lattice. For bulk magnesium $a = b = 3.21 \text{ \AA}$ and $c = 5.21 \text{ \AA}$ [42].

TABLE I: The averaged values of the primitive axes and its ratio for the hcp lattice element for magnesium clusters with $N = 17$ calculated within the B3PW91 approximation. Values in brackets correspond to singly-charged magnesium clusters.

| | $M g_{17}$ | $M g_{18}$ | $M g_{19}$ | $M g_{20}$ | $M g_{21}$ | $M g_{\text{bulk}}$, [42] |
|----------------------|-------------|-------------|-------------|-------------|-------------|----------------------------|
| $h_{ci}, \text{\AA}$ | 4.87 (4.93) | 4.94 (4.55) | 5.03 (5.05) | 5.32 (5.22) | 5.31 (5.19) | 5.21 |
| $h_{ai}, \text{\AA}$ | 3.21 (3.20) | 3.14 (3.19) | 3.26 (3.24) | 3.06 (3.11) | 3.06 (3.12) | 3.21 |
| h_{ci}/h_{ai} | 1.52 (1.54) | 1.57 (1.43) | 1.54 (1.56) | 1.74 (1.68) | 1.73 (1.66) | 1.62 |

The ground state geometries of the cationic magnesium clusters are not very different from those obtained for the neutral parent clusters with the exception of $M g_3^+$ and $M g_4^+$, the equilibrium geometries of which are linear chains. Below, we discuss the stability of the linear chain isomers for the magnesium clusters (neutral and singly-charged) within the size range considered.

In figure 4, we present the average bonding distance, h_{di} , calculated within the B3PW91 approximation for neutral and singly-charged magnesium clusters. When calculating the

average bonding distance in a cluster, interatomic distances smaller than 4.1 Å have only been taken into account. The bulk limit for the magnesium hcp lattice [42] indicated in figure by horizontal dashed line.

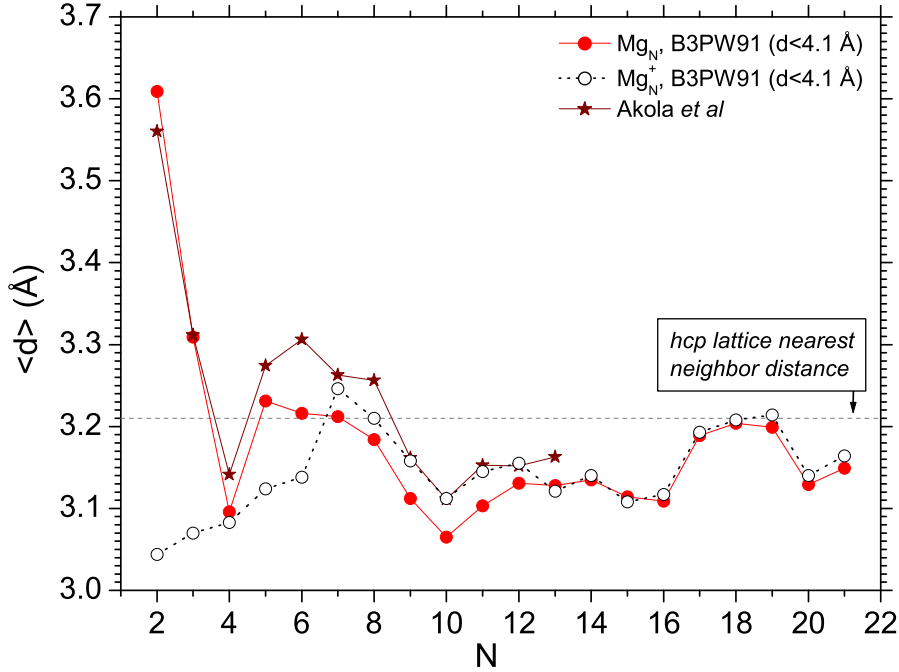


FIG. 4: The average bonding distance as a function of cluster size for neutral and singly-charged magnesium clusters. Stars present the results of the work by Akola et al [27]. The horizontal dashed line indicates the bulk limit for the hcp lattice [42].

Figure 4 shows how the average bonding distance evolves with increasing cluster size. It is clearly seen that the dependence of the average bonding distance on cluster size has essentially non-monotonic oscillatory behavior. For Mg_2 , the bonding distance calculated within the B3PW91 method is equal to 3.609 Å, which is in a good agreement with the experimental result 3.891 Å of Ref. [39]. The appearance of deep minima in the size dependence of the average bonding distance shows that Mg_4 , Mg_{10} , and Mg_{20} clusters (8, 20 and 40 valence electrons, respectively) are more tightly packed than their neighbours. This behavior can be interpreted by the influence of electronic shell effects on the geometric structure of magnesium clusters. It supports the conclusion of Ref. [44] that electronic shell effects can enhance the stability of geometric structures resulting from dense ionic packing.

A significant step-like increase in the average bonding distance happens at the transition from Mg_{16} to Mg_{17} cluster. As we have discussed above this transition is accompanied by a considerable re-arrangement of the cluster geometry. Indeed, starting from the Mg_{17} cluster the three-layered trigonal prism is formed, as it is shown in figure 1. The Mg_{17} cluster has 34 valence electrons which form the closed shell electronic structure, according to the spherical jellium model. Therefore, it is natural to assume that namely electronic shells effects induce the structural re-arrangement in the Mg_{17} cluster that happens to be the turning-point in the formation of the hcp lattice form magnesium. It is clearly seen in figure 4 that the average bonding distance for magnesium clusters approaches the bulk limit for $N = 17$, with an exception of the Mg_{20} cluster, which is more compact due to the electronic shell closure.

The evolution of the average bonding distance with cluster size differs for magnesium clusters from that for sodium. For neutral sodium clusters, one can see odd-even oscillations of hdi atop its systematic growth and approaching the bulk limit [22]. These features have the quantum origin and arise due to the spin coupling of the delocalized valence electrons. For magnesium clusters, the average bonding distance depends on size non-monotonically, with minima for the Mg_4 , Mg_{10} , and Mg_{20} clusters, as well as with the considerable step-like increase for the Mg_{17} cluster. Such an irregular behavior is induced by the closure of electronic shells of the delocalized electrons.

Manifestation of the magic numbers in the dependence of the average bonding distance on cluster size coinciding with the spherical jellium model magic numbers does not imply, however, the rapid metallization of magnesium clusters. To investigate the transition of van der Waals to metal bonding in magnesium clusters it is necessary to explore in detail the evolution of their electronic properties. Below we perform such analysis in detail.

Dashed line in figure 4 shows the average bonding distance as a function of cluster size calculated for singly-charged magnesium clusters. Figure 4 demonstrates the essential difference in the cluster size dependence of hdi for the cationic and neutral magnesium clusters with $N = 6$. The small cationic magnesium clusters are more compact in comparison with the corresponding neutral clusters. For example, for Mg_2^+ the bonding distance is equal to 3.044 Å, which is much less than in the case of Mg_2 . This phenomenon has a simple physical explanation: the removed electron is taken from the antibonding orbital. The fact that cationic magnesium clusters are more stable than the parent neutral and anionic clusters has been already noted in [24].

Within the size range $7 \leq N \leq 12$, the average bonding distances for single-charged and neutral magnesium clusters behave similarly although the absolute value of hdi for neutral clusters remains slightly larger. For $N \geq 13$, the bonding distances hdi for neutral and singly-charged cationic magnesium clusters become almost identical.

Figure 4 demonstrates the good agreement of our results with the dependence of hdi on N calculated in [27] for neutral magnesium clusters within the size range $N \leq 13$.

B. Binding energy per atom for $M g_N$ and $M g_N^+$ clusters.

The binding energy per atom for small neutral and singly-charged magnesium clusters is defined as follows:

$$E_b = N = E_1 \quad E_N = N \quad (1)$$

$$E_b^+ = N = (N - 1)E_1 + E_1^+ \quad E_N^+ = N ; \quad (2)$$

where E_N and E_N^+ are the energies of a neutral and singly-charged N-particle atomic cluster, respectively. E_1 and E_1^+ are the energies of a single magnesium atom and an ion.

Figures 5 and 6 show the dependence of the binding energy per atom for neutral and singly-charged clusters as a function of cluster size. The energies of clusters have been obtained using the B3LYP, B3PW91 and MP4 methods. Calculations of the binding energies have been performed by different theoretical methods and with the use of different exchange-correlation functionals for the sake of comparison of their accuracy and computation efficiency. In figure 5 filled rhombus, crossed rhombus and opened pentagons show the result of calculations by Kumar et al [25], Reuse et al [24] and Delaly et al [26] respectively. These calculations have been performed within the Hohenberg-Kohn-Sham local-density approximation using the Perdew and Zunger [45] parameterization of the Ceperley and Alder [46] data for the exchange correlations. Crossed circles and stars present the results of Delaly et al [26] and Akola et al [27] derived with the use of the gradient-corrected approximation [47, 48] and the PBE parameterization of the gradient-corrected exchange-correlation energy functional [49] respectively.

Figure 5 shows that, although, the qualitative behavior of the binding energy per atom calculated within different approaches is similar, the quantitative discrepancy between the curves is rather considerable. This is a result of different accounting for the gradient cor-

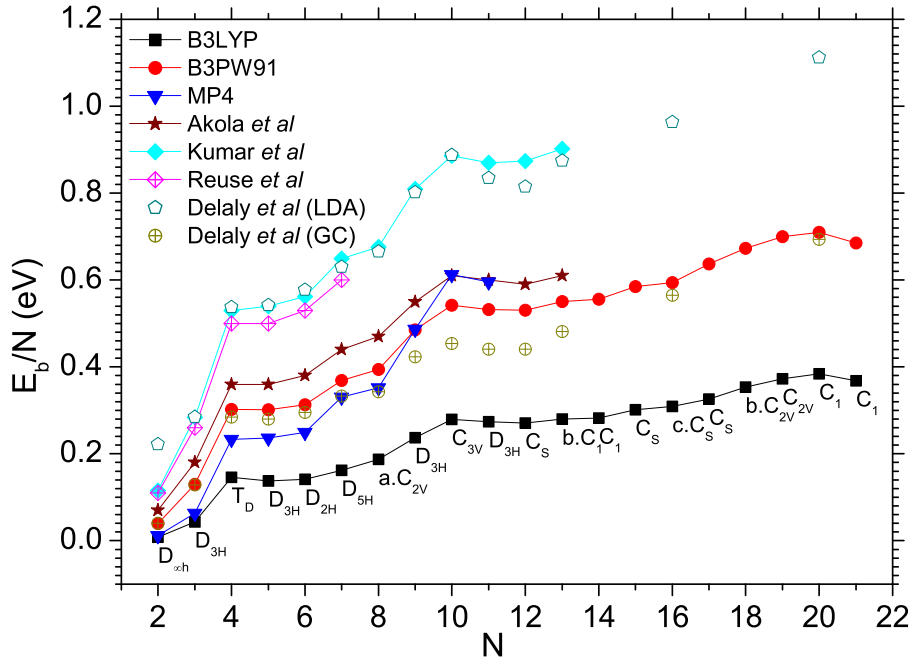


FIG . 5: Binding energy per atom for neutral magnesium clusters as a function of cluster size. Squares, circles and lower triangles represent the binding energies per atom calculated by the B3LYP, B3PW91 and MP4 methods respectively. Stars, filled rhombus and crossed rhombus show the results of the works by Akola et al [27], Kumar et al [25], and Reuse et al [24] respectively. Opened pentagons and crossed circles show the result of Delaly et al [26] obtained with the use of the LDA and gradient-corrected (GC) LDA methods respectively. Labels indicate the point symmetry group of the isomers represented. Their geometries one can find in section IIIA .

rections to the local-density exchange correlation interaction within different methods. The gradient corrections have been shown to provide a systematic improvement in the computed properties of magnesium clusters [26]. The difference in the binding energy per atom for neutral magnesium clusters with $N = 21$ calculated with the use of the gradient-corrected B3LYP and B3PW91 methods reaches 0.35 eV. The reason for this difference is in the different way of accounting for many-electron correlations within the B3LYP and B3PW91 methods. To explore what type of parameterization of the exchange-correlation energy is more reliable for magnesium clusters we have used the post-Hartree-Fock Muller-Plesset perturbation theory. This method is free of phenomenological parameters and can be used

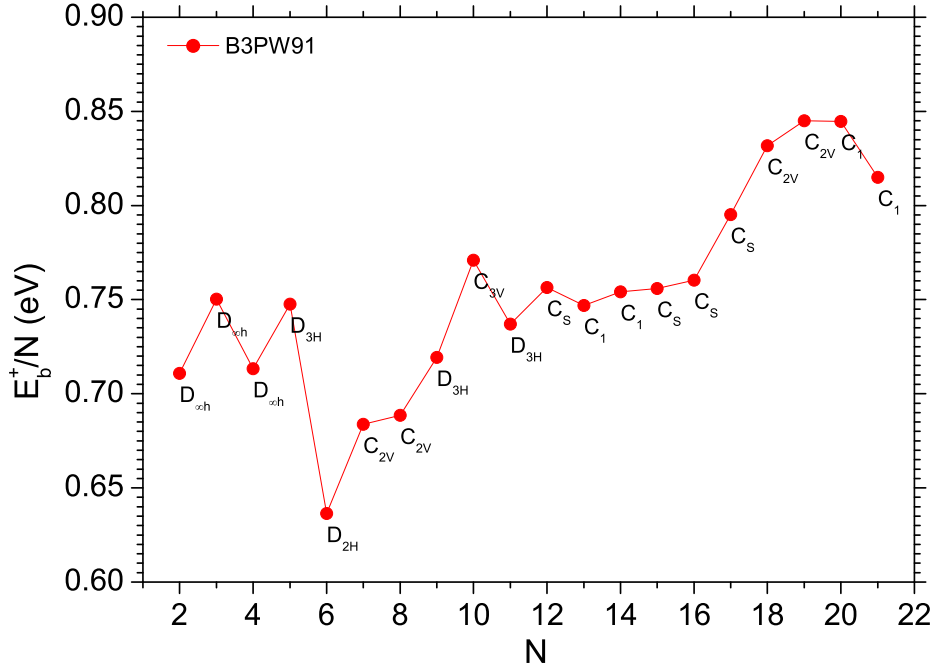


FIG . 6: The same as in Fig.5 but for singly-charged magnesium clusters.

as a criterion for checking the reliability of various density-functional theory schemes. The disadvantage of the perturbation theory approach consists in the fact that it leads to the dramatic growth of the computational costs with increasing the number of electrons in the system in comparison with that for the density-functional theory calculations. Therefore, we have used the MP4 method only for clusters with the number of atoms $N = 11$.

Figure 5 shows that the results of the MP4 theory are in a reasonable agreement with those derived by the B3PW91 method. This comparison demonstrates that for magnesium clusters simulations the B3PW91 method is more reliable than the B3LYP one. Our results derived within the B3PW91 and MP4 approximations are in a good agreement with those from Ref. [26, 27].

We now discuss the behavior of the binding energy as a function of cluster size for both neutral and singly-charged magnesium clusters. For neutral magnesium clusters, the binding energy per atom increases steadily with the growth cluster size. The local maximum of $E_b = N$ at $N = 4, 10$ and 20 correspond to the most stable configurations of the magic magnesium clusters possessing $N_{el} = 8, 20$ and 40 valence electrons respectively. This behavior is in

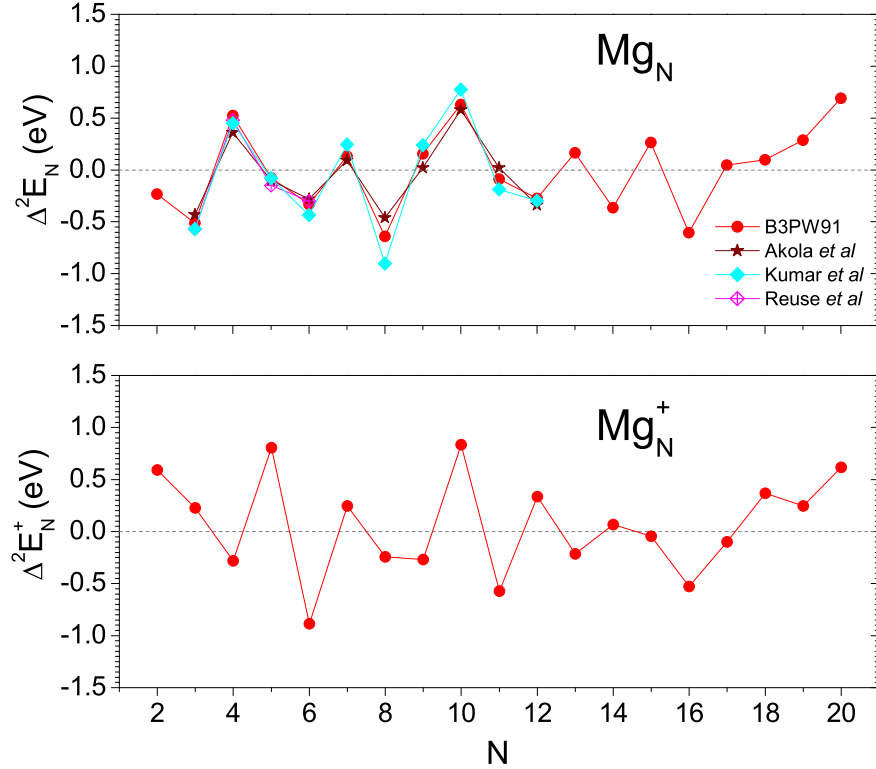


FIG . 7: Second differences of total energy for neutral, $\Delta^2 E_N = E_{N+1} - 2E_N + E_{N-1}$, and singly-charged, $\Delta^2 E_N^+ = E_{N+1}^+ - 2E_N^+ + E_{N-1}^+$, magnesium clusters. Stars show the result of the work by Akola et al [27], filled rhombus by Kumar et al [25], and crossed rhombus by Reuse et al [24].

agreement with the simple spherical jellium model. The analysis of the second differences of the binding energy (see Fig.7) confirms this conclusion and makes a hint about relative stability of the Mg_5 , Mg_7 , Mg_9 , Mg_{11} , Mg_{13} , Mg_{15} , Mg_{17} – Mg_{19} clusters, in addition to the magic clusters Mg_4 , Mg_{10} and Mg_{20} . The additional magic numbers can be explained within the deformed jellium model accounting for spheroidal deformations of the cluster core (see, e.g., [16, 17, 18] and references therein). For a spheroidal jellium cluster, the orbital angular momentum does not remain a good quantum number characterizing the valence electrons energy levels. In this case, the energy levels are characterized by the projection of the angular momentum on the principal axis and by the parity of the wave function. Thus, the energy levels with $\ell = 0$ are twofold degenerated on the projection of the electron's spin, while those with $\ell \neq 0$ are fourfold degenerated both on the projection

of the electron spin and on the sign of the projection on the principal cluster axis. The deformed jellium clusters having closed electronic subshells possess the enhanced stability. Therefore, in addition to the spherical magic clusters with 8, 20, 40 etc valence electrons, the deformed jellium clusters with 6, 10, 14, 18, 22, 26, 30, 34, 36 etc. valence electrons turn out to be relatively stable. This fact leads to the following additional magic numbers 3, 5, 7, 9, 11, 13, 15, 17, 18 for the jellium magnesium clusters. Some of these numbers, such as 3, 5, 9, 11 precede or follow the spherical magic numbers 4, 10, 20 and as a result of that become masked and are not that pronounced in the second differences analysis.

For singly-charged magnesium clusters, the binding energy per atom as a function of cluster size is essentially non-monotonic in the region $N = 13$. At larger N , it grows monotonously up to $N = 20$. The local maxima of the binding energy for the Mg_3^+ , Mg_5^+ , Mg_{10}^+ , Mg_{12}^+ , Mg_{19}^+ and Mg_{20}^+ clusters indicate their enhanced stability. Figure 7 shows second differences of the total energy for singly-charged magnesium clusters. This figure demonstrates the enhanced stability of the mentioned cluster ions and a few additional singly-charged magnesium clusters Mg_7^+ , Mg_{14}^+ , Mg_{15}^+ and Mg_{18}^+ .

The sequence of magic numbers for singly charged magnesium clusters differs from that for neutral clusters. This happens because singly charged magnesium clusters always possess odd number of valence electrons and, thus, always contain open electronic shells. For neutral magnesium clusters, situations of both close and open electronic shells are possible. The enhanced stability of a Mg -cluster ion arises, when its electronic configuration has one hole in or an extra electron above the filled shells. Thus, the cluster ions Mg_5^+ , Mg_{11}^+ and Mg_{21}^+ contain one extra electron over the completed spherical electronic shells, while the clusters Mg_4^+ , Mg_{10}^+ and Mg_{20}^+ have a hole in the spherical outer electronic shell. Our results presented in figures 6 and 7 demonstrate that the cluster ions Mg_5^+ , Mg_{10}^+ and Mg_{20}^+ turn out to be more stable than their neighbors. We note that the alteration of the magic number from $N = 4$ for neutral Mg -clusters to $N = 5$ for Mg -cluster ions happens because the electronic configuration containing an extra electron becomes more favorable for Mg_5^+ . This is not the case for the Mg_{10}^+ and Mg_{20}^+ clusters, those outer electronic configurations contain a hole.

The Mg -cluster mass spectra have been recorded in [29] indicating the enhanced stability of the clusters with $N = 5, 10, 15, 18$ and 20 . In that work the role of the cluster ionization was not reliably clarified [29] and thus the charge state of the clusters was not reliably

determined. As a result, the observed magic numbers sequence should be a combination of the magic numbers sequences for neutral and singly-charged cluster ions. Thus, $N = 5$ is the ionic magic number, $N = 10, 18$ and 20 are the magic numbers manifesting themselves clearly for both neutral Mg -clusters and Mg -cluster ions, $N = 15$ is the neutral magic cluster number. The experimentally observed enhancement of the mass spectrum in the region $17 \leq N \leq 20$ corresponds to the positive values of 2E_N in this region of N derived in our calculations. The second differences are positive and relatively large for $N = 13$ (neutral clusters) and $N = 12$ (singly-charged cluster ions). Possibly, the interplay between neutral clusters and ions make these numbers masked in experiment. The second differences are also positive for $N = 7$ for neutral Mg -clusters and for $N = 3$ and 7 for Mg -cluster ions, although the enhancement for those numbers have not been experimentally observed. We explain this fact by possible suppression of the experimental signal in the region of small N and relatively small values of the second differences in the mentioned cases.

The potential energy surface for a cluster becomes more and more complicated with increasing cluster size. The magnesium clusters are not an exception. Figure 8 demonstrates this fact where we present the binding energies per atom calculated for a variety of isomers of neutral magnesium clusters. The corresponding point symmetry groups and the accurate values of the total energies calculated within the B3LYP and B3PW91 approximations are presented in Appendix in tables II and III respectively. Most of the isomer configurations have been obtained using the B3LYP method, while the B3PW91 method has been used for the exploration of the ground state energy isomers, as well as for the linear and ring-like isomer structures.

Squares in figure 8 correspond to the most stable clusters possessing the minimal total energy. Among the variety of isomers, presented in figure 8, we mark certain groups of isomers with the fixed symmetry. So, circles present the linear chains (D_{1h} point symmetry group) and the upper triangles correspond to the rings of N atoms (D_{Nh} point symmetry group). It is an interesting fact that among the multitude of the isomers of neutral magnesium clusters the linear chains and rings are always stable. We pay a particular attention to these structures because of their possible applications in nano-technology. Extracting these isomers and putting them on a substrate one can produce one-atom wide quantum wires. The linear chains and rings of atoms are also very interesting from the theoretical point of view, because with their help one can investigate the transition from one- to

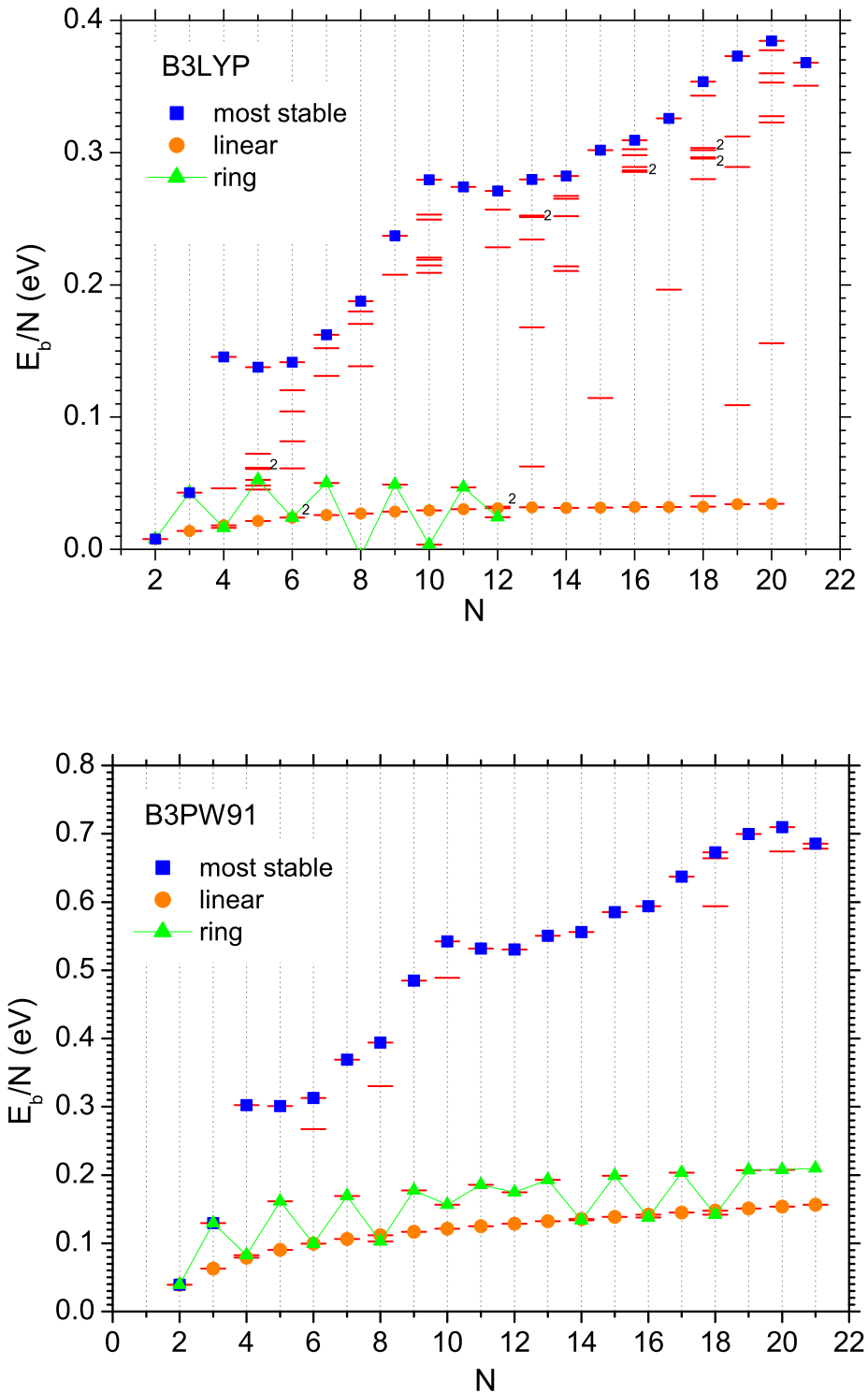


FIG . 8: Binding energy per atom for a variety of isomers of neutral magnesium clusters as a function of cluster size. The corresponding point symmetry groups and the accurate values of the total energies are presented in Appendix in tables II and III. Numbers near some lines show the number of found isomers with the corresponding close energies.

two-dimensional structures. For linear chains, the binding energy per atom increases slowly with the growth the number of atoms, while in the case of rings the value of $E_b=N$ has the prominent odd-even oscillatory behavior.

This behavior arises as a result of successive filling the π - and π -symmetry orbitals by valence electrons in magnesium linear chains and rings. Indeed, because of its symmetry the one-dimensional linear chain of N magnesium atoms has the following configuration of valence electrons: $1^2, 2^2, 3^2, \dots, N^2$. Therefore for any N it has the closed electronic shell structure. This fact explains the monotonous growth with N of the linear chain binding energy, and its relative saturation in the region $N > 10$.

The molecular orbitals for the structure of the ring-type have to be aligned with the plane of the ring. Such orbitals are fourfold degenerated due to symmetry reasons. The Mg_2 dimer has four valence electrons that occupy spherically-shaped 1^2 and prolate-like 2^2 orbitals. The Mg_3 trimer has six valence electrons, two of them occupy 1^2 state, while the remaining four electrons fill the fourfold degenerated 1^4 orbital aligned with the plane of the trimer. With increasing the number of magnesium atoms in the ring, the valence electrons continue to occupy fourfold degenerated orbitals aligned with the plane of the ring. Therefore, in the magnesium ring-like isomers with the odd number of atoms all electronic shells are closed, while the isomers with the even number of atoms have the open electronic shell. This fact results in the enhanced stability of the magnesium rings with an odd number of atoms $N = 3; 5; 7; 9; \dots$ etc. and explains the odd-even oscillatory behavior of the binding energy for the magnesium rings.

C. Ionization potentials and HOMO-LUMO gaps

Let us now consider how the ionization potential of magnesium clusters evolves with increasing cluster size. The ionization potential of a cluster V_i is equal to the difference between the energies of the corresponding cluster ion and the neutral cluster, $V_i = E_N^+ - E_N$. Figure 9 shows the dependence of the adiabatic V_i^{adiab} (i.e. the geometry relaxation of the ionized cluster is taken into account) and vertical V_i^{vert} (i.e. the cluster geometry is frozen during the ionization process) ionization potential on N . We compare our results derived by the B3PW91 method with theoretical data from Ref. [27] and [24] and with the bulk limit, $V_i^{\text{bulk}} = 3.64$ eV, taken from [42].

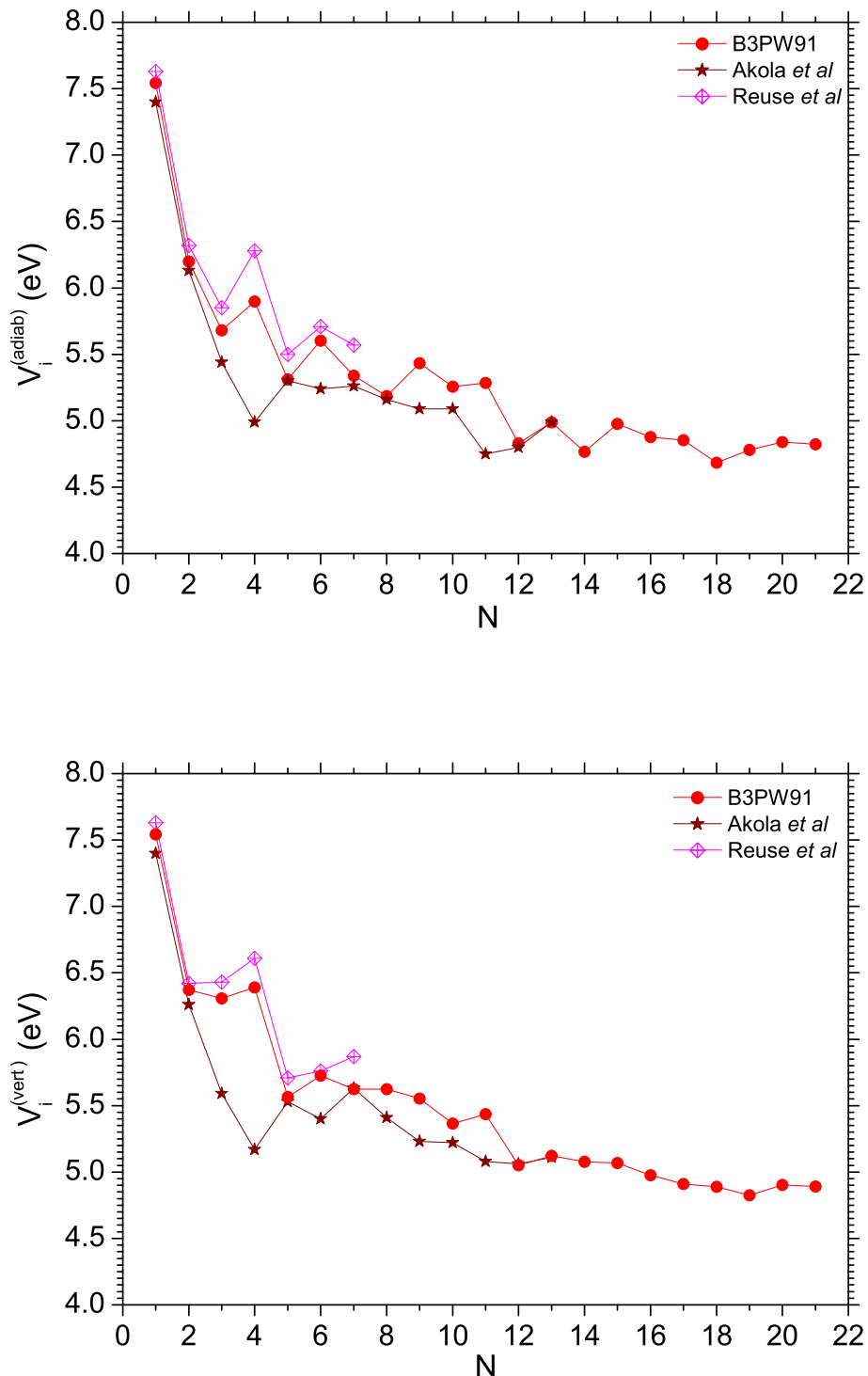


FIG. 9: Adiabatic, $V_i^{(\text{adiab})}$, and vertical, $V_i^{(\text{vert})}$, ionization potential for small magnesium clusters. Stars and crossed rhombus show the result of the work by Akola *et al* [27] and by Reuse *et al* [24] respectively.

Both the vertical and adiabatic ionization potentials evolve non-monotonously with increasing cluster size. Figure 9 shows that ionization potential of magnesium clusters steadily but rather slow decreases towards the bulk limit. This evolution is neither rapid nor monotonous process. In order to exclude the influence of the cluster geometry rearrangement, we first consider the vertical ionization potential. The size dependence of the vertical ionization potential has a prominent maximum at $N = 4$ followed by a sharp decrease. Such a behavior of the ionization potential is typical for the jellium model, predicting maxima in the size dependence of the ionization potential at the magic numbers corresponding to the clusters with closed electronic shells. Our data are in a good agreement with the results of Ref. [24], but contradict to those reported in Ref. [27] for the Mg_3 and Mg_4 clusters. In [27] the appearance of the deep minimum in vertical ionization potential at $N = 4$ was explained as a result of a stronger charge delocalization in the Mg_4 cluster in comparison with its neighbours.

We note that the peculiarities in the ionization potential dependence on N correlate with the magic numbers that appear for the singly-charged magnesium clusters. Indeed, the minima in V_i^{vert} correspond to the maxima in $E_b^+ = N$ for Mg -cluster ions (see Fig. 6). This fact has a simple explanation. The ionization potential of a cluster is equal to the difference between the energies of the corresponding cluster ion and the neutral cluster. For neutral Mg -clusters, the binding energy as a function of N increases steadily with the growth cluster size, while for Mg -cluster ions – irregularly. Thus, their difference includes all the irregularities that appear in the binding energy dependence on N for singly-charged magnesium clusters.

For $N = 6$, the vertical ionization potential changes slowly with increasing cluster size. This process is characterized by the irregularities that originate due to the influence of the cluster geometry on the jellium-type electronic structure of Mg -clusters.

Indeed, the shape of a jellium cluster is defined by its electronic structure. Thus, the closed shell jellium clusters are spherical, while clusters with opened electronic shells are deformed due to the Jahn-Teller distortions. The jellium picture works fairly well for sodium clusters. The ionization potential of sodium clusters drops rapidly and systematically at the electronic shell closures. The N -dependence of the ionization potential has prominent, regular odd-even oscillations (see, e.g., [18, 22] and references therein). Magnesium clusters are different. As discussed in section IIIA, the evolution of the Mg -cluster geometry is closely

connected with the formation of elements of the hcp lattice cell. Although, the electronic shell effects clearly manifest themselves in the formation of the Mg-cluster geometry, they do not determine it completely. In other words, there is an interplay of the jellium and the hcp lattice factors in the formation of the Mg-cluster geometry and the electronic properties such as the binding energy and the ionization potential.

The adiabatic ionization potential dependence that is shown in figure 9 exhibits qualitatively the same behavior as the vertical one, however, has more pronounced irregularities due to geometry rearrangements of the ionized clusters.

Figure 10 shows the gap E_g between the highest occupied and the lowest unoccupied molecular orbitals (HOMO-LUMO gap) for the Mg-clusters as a function of cluster size. For the sake of comparison, we have also calculated the HOMO-LUMO gap for the sodium clusters and present it in figure 10. Calculations have been performed using the B3PW91 and B3PLYP methods. The geometries of neutral sodium clusters have been taken from [22]. For the small magnesium clusters with $N = 13$, we compare our results with those presented in Ref. [27].

The size dependence of E_g for neutral sodium clusters has an oscillatory behavior with local maximum at $N = 6, 8, 10, 14$ and 20 . These maxima correspond to the electronic shell closures in a full accordance with the deformed jellium model. The local maximum in the size dependence of E_g at $N = 12$ and the shift of the local maximum from $N = 18$ to $N = 17$ are the consequences of triaxial deformations [22]. Thus, the triaxial deformation leads to the splitting of the fourfold degenerated highest occupied orbital on two twofold degenerated orbitals. As a result of that the additional shell closure at the $N_{el} = 12$ appears.

For Mg-clusters, the evolution of the HOMO-LUMO gap with the growth cluster size differs from that for Na-clusters. The gap E_g calculated for magnesium clusters shows the oscillatory behavior accompanied by the gradual decrease in the absolute value. Maxima in this dependence have different origin. Thus, the increase of E_g at $N = 4, 10$ and 20 correspond to the magic numbers of the spherical jellium model ($N_{el} = 8, 20$ and 40 respectively). The similar feature also does exist for Na-clusters at $N = 8$ and 20 . The drop in E_g at $N = 8, 11$ and 16 is the result of the significant structural change, which we observe for Mg-clusters at those numbers.

As discussed in section IIIA, the basic element of the Mg-cluster geometry for $N = 8$ is pyramidal. Starting from Mg₉ the new element, namely the six atom trigonal prism,

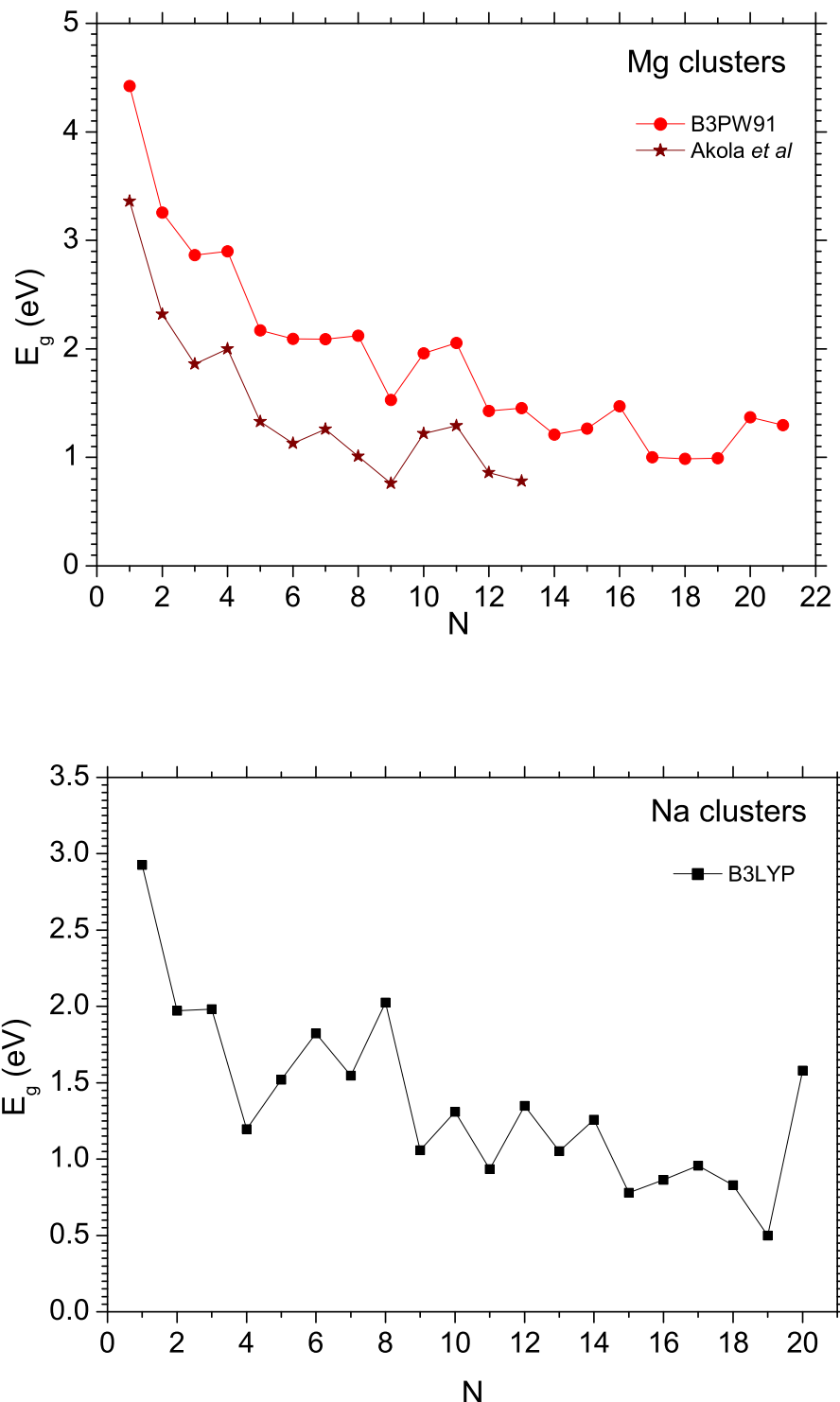


FIG . 10: Gap between the highest occupied and the lowest unoccupied eigenstates for the Mg and Na clusters as a function of cluster size. Circles and squares represent the HOMO-LUMO gap calculated by the B3PW91 and the B3LYP methods respectively. Stars show the result of the work by Akola *et al* [27].

determines the M_g -cluster structure. The prominent structural change arises at $N = 12$, when the high symmetry of the system reduces to the point symmetry group C_s . For $N = 17$ another motif based on the three-layered trigonal prism dominates the cluster growth.

The analysis of the HOMO-LUMO gap evolution for M_g clusters supports our conclusion on the role of the interplay of the jellium and hcp lattice factors in the formation of M_g cluster properties.

We note that the HOMO-LUMO gap remains rather large even for the clusters with $N = 17$ possessing elements of the hcp lattice of the bulk M_g . This fact confirms the conclusion on the slow and non-monotonic evolution of metallic properties in M_g clusters.

IV. CONCLUSION

The optimized geometries and electronic properties of neutral and singly-charged magnesium clusters consisting of up to 21 atoms have been investigated using the B3PW91, B3LYP and MP4 methods accounting for all electron in the system. The detailed comparison of the results of the phenomenological B3PW91 and B3LYP density-functional methods with the results of the systematic ab initio post-Hartree-Fock many-body theory leads us to the conclusion that the B3PW91 method is more reliable for M_g -cluster simulations than the B3LYP one.

We have investigated the size evolution of the M_g -clusters geometry. It has been shown that starting from $M_{g_{17}}$ the three-layered trigonal prism structure determines the cluster growth, which is the basic element of the hcp lattice for the bulk magnesium.

We have investigated the electronic properties of magnesium clusters. It has been shown that the electronic shell effects and jellium-like behavior clearly manifest themselves in the formation of geometrical properties, however, the shell effects do not determine the geometry of M_g clusters completely. We have demonstrated that due to the interplay of the jellium and the hcp lattice factors the electronic properties of magnesium clusters possess irregularities which can not be explained within the simple jellium model. It has been shown that the metallic evolution of magnesium clusters is slow and non-monotonic process.

The results of this work can be extended in various directions. One can use the similar methods to study structure and properties of various types of clusters. It is interesting to extend calculations towards larger cluster sizes and to perform more advanced comparison

of model and *ab initio* approaches. A lot of novel problems arise, when considering collisions and electron excitations in the clusters with the optimized geometries [21]. These and many more other problems on atomic cluster physics can be tackled with the use of methods considered in our work.

Acknowledgments

The authors acknowledge support from the Alexander von Humboldt Foundation and the Russian Academy of Sciences (Grant 44).

APPENDIX

TABLE II: Total energies and the point symmetry groups for a variety of isomers of neutral magnesium clusters. Calculations have been done by the B3LYP method.

| N | Point group | Energy (a.u.) | N | Point group | Energy (a.u.) | N | Point group | Energy (a.u.) |
|---|------------------|---------------|----|------------------|---------------|----|------------------|---------------|
| 1 | | -200.0931 | 9 | D _{1h} | -1800.8472 | 16 | cC _s | -3201.6713 |
| 2 | D _{1h} | -400.1868 | 10 | C _{3v} | -2001.0336 | | bC ₁ | -3201.6673 |
| 3 | D _{3h} | -600.2840 | | C _{4v} | -2001.0239 | | aC ₁ | -3201.6646 |
| | D _{1h} | -600.2807 | | T _d | -2001.0225 | | T _d | -3201.6594 |
| 4 | T _d | -800.3938 | | C ₁ | -2001.0120 | | aC _s | -3201.6579 |
| | D _{2h} | -800.3792 | | D _{3h} | -2001.0114 | | bC _s | -3201.6572 |
| | D _{1h} | -800.3750 | | C _{2v} | -2001.0098 | | D _{1h} | -3201.5082 |
| | D _{4h} | -800.3748 | | D _{4d} | -2001.0078 | 17 | C _s | -3401.7861 |
| 5 | D _{3h} | -1000.4907 | | D _{1h} | -2000.9417 | | D _{3h} | -3401.7052 |
| | C _{4v} | -1000.4787 | | D _{10h} | -2000.9322 | | D _{1h} | -3401.6026 |
| | T _d | -1000.4768 | 11 | D _{3h} | -2201.1348 | 18 | bC _{2v} | -3601.9095 |
| | C _{2v} | -1000.4766 | | D _{11h} | -2201.0430 | | cC _s | -3601.9026 |
| | D _{5h} | -1000.4751 | | D _{1h} | -2201.0362 | | C ₂ | -3601.8764 |
| | D _{2D} | -1000.4743 | 12 | aC _s | -2401.2366 | | bC _s | -3601.8752 |
| | D _{2h} | -1000.4738 | | bC _s | -2401.2304 | | aC _s | -3601.8716 |
| | D _{1h} | -1000.4694 | | C _{2v} | -2401.2178 | | aC _{2v} | -3601.8711 |
| 6 | D _{2h} | -1200.5897 | | D _{6h} | -2401.1313 | | D _{5h} | -3601.8608 |
| | D _{4h} | -1200.5851 | | D _{1h} | -2401.1308 | | D _{6h} | -3601.7022 |
| | C _{5v} | -1200.5815 | | D _{12h} | -2401.1278 | | D _{1h} | -3601.6970 |
| | D _{3h} | -1200.5765 | 13 | bC ₁ | -2601.3438 | 19 | C _{2v} | -3802.0292 |
| | O _h | -1200.5720 | | C _s | -2601.3308 | | C _{3v} | -3801.9867 |
| | D _{6h} | -1200.5639 | | aC ₁ | -2601.3302 | | D _{5h} | -3801.9706 |
| | D _{1h} | -1200.5638 | | C _{3v} | -2601.3221 | | D _{6h} | -3801.8449 |
| 7 | D _{5h} | -1400.6933 | | I _h | -2601.2904 | | D _{1h} | -3801.7925 |
| | C ₃ | -1400.6908 | | D _{6h} | -2601.2401 | 20 | C ₁ | -4002.1444 |
| | C _{3v} | -1400.6854 | | D _{1h} | -2601.2253 | | dC _{2v} | -4002.1392 |
| | D _{7h} | -1400.6645 | 14 | C ₁ | -2801.4485 | | cC _{2v} | -4002.1263 |
| | D _{1h} | -1400.6583 | | bC _{3v} | -2801.4397 | | bC _{2v} | -4002.1212 |
| 8 | aC _{2v} | -1600.7999 | | C _s | -2801.4407 | | T _d | -4002.1026 |
| | C _s | -1600.7976 | | C _{2v} | -2801.4328 | | aC _{2v} | -4002.0990 |
| | bC _{2v} | -1600.7948 | | O _h | -2801.4115 | | D _{6h} | -4001.9764 |
| | T _d | -1600.7854 | | aC _{3v} | -2801.4134 | | D _{1h} | -4001.8870 |
| | D _{1h} | -1600.7527 | | D _{1h} | -2801.3194 | 21 | C ₁ | -4202.2389 |
| 9 | D _{3h} | -1800.9162 | 15 | C _s | -3001.5627 | | C _{2v} | -4202.2255 |
| | C _{3v} | -1800.9064 | | D _{6h} | -3001.4594 | | | |
| | D _{9h} | -1800.8540 | | D _{1h} | -3001.4138 | | | |

TABLE III: The same as table II but for the P 3P W 91 method.

| N | Point group | Energy (a.u.) | N | Point group | Energy (a.u.) |
|----|-------------|---------------|----|-------------|---------------|
| 1 | | -200.0379 | 14 | C_1 | -2800.8170 |
| 2 | D_{1h} | -400.0788 | | D_{1h} | -2800.6007 |
| 3 | D_{3h} | -600.1281 | | D_{14h} | -2800.5997 |
| | D_{1h} | -600.1207 | 15 | C_s | -3000.8914 |
| 4 | T_d | -800.1962 | | D_{15h} | -3000.6786 |
| | D_{4h} | -800.1638 | | D_{1h} | -3000.6453 |
| | D_{1h} | -800.1633 | 16 | cC_s | -3200.9560 |
| 5 | D_{3h} | -1000.2450 | | D_{1h} | -3200.6902 |
| | D_{5h} | -1000.2193 | | D_{16h} | -3200.6880 |
| | D_{1h} | -1000.2063 | 17 | C_s | -3401.0428 |
| 6 | D_{2h} | -1200.2966 | | D_{17h} | -3400.7719 |
| | C_{5v} | -1200.2865 | | D_{1h} | -3400.7353 |
| | D_{6h} | -1200.2495 | 18 | bC_{2v} | -3601.1279 |
| | D_{1h} | -1200.2495 | | cC_s | -3601.1221 |
| 7 | D_{5h} | -1400.3604 | | bC_s | -3601.0756 |
| | D_{7h} | -1400.3091 | | D_{1h} | -3600.7806 |
| | D_{1h} | -1400.2928 | | D_{18h} | -3600.7766 |
| 8 | aC_{2v} | -1600.4193 | 19 | C_{2v} | -3801.2093 |
| | T_d | -1600.4005 | | D_{19h} | -3800.8653 |
| | D_{1h} | -1600.3364 | | D_{1h} | -3800.8260 |
| | D_{8h} | -1600.3335 | 20 | C_1 | -4001.2801 |
| 9 | D_{3h} | -1800.5018 | | bC_{2v} | -4001.2539 |
| | D_{9h} | -1800.4000 | | D_{20h} | -4000.9111 |
| | D_{1h} | -1800.3800 | | D_{1h} | -4000.8716 |
| 10 | C_{3v} | -2000.5786 | 21 | C_1 | -4201.3255 |
| | T_d | -2000.5590 | | C_{2v} | -4201.3201 |
| | D_{10h} | -2000.4367 | | | |
| | D_{1h} | -2000.4238 | | | |
| 11 | D_{3h} | -2200.6322 | | | |
| | D_{11h} | -2200.4923 | | | |
| | D_{1h} | -2200.4678 | | | |
| 12 | aC_s | -2400.6891 | | | |
| | D_{12h} | -2400.5321 | | | |
| | D_{1h} | -2400.5119 | | | |
| 13 | bC_1 | -2600.7561 | | | |
| | D_{13h} | -2600.5853 | | | |
| | D_{1h} | -2600.5562 | | | |

References

[1] W. D. Knight, K. Clemenger, W. A. de Heer, W. A. Saunders, M. Y. Chou and M. L. Cohen, *Phys. Rev. Lett.* 52, 2141 (1984).

[2] C. Bréchignac, Ph. Cahuzac, F. Carlier, J. Leygnier, *Chem. Phys. Lett.* 164, 433 (1989).

[3] K. Selby, M. Vollmer, J. Masui, V. Kresin, W. A. de Heer and W. D. Knight, *Phys. Rev. B* 40, 5417 (1989).

[4] K. Selby, V. Kresin, J. Masui, M. Vollmer, W. A. de Heer, A. Scheidemann, W. D. Knight, *Phys. Rev. B* 43, 4565 (1991).

[5] A. Hergert, S. Kuckeberg, L. Schweikhard, M. Vogel, C. Walther, *Physica Scripta T* 80, 200 (1999).

[6] W. Ekardt (ed.), *Metal Clusters* (Wiley, New York, 1999).

[7] *Atomic Clusters and Nanoparticles*, NATO Advanced Study Institute, les Houches Session LXXIII, les Houches, 2000, edited by C. Guet, P. Hobza, F. Spiegelman and F. David (EDP Sciences and Springer Verlag, Berlin, 2001).

[8] W. A. de Heer, *Rev. Mod. Phys.* 65, 611 (1993).

[9] M. Brack, *Rev. Mod. Phys.* 65, 677 (1993).

[10] C. Bréchignac, J.-P. Connerade, *J. Phys. B: At. Mol. Opt. Phys.* 27, 3795 (1994).

[11] H. Haberland (ed.), *Clusters of Atoms and Molecules, Theory, Experiment and Clusters of Atoms*, (Springer Series in Chemical Physics, Berlin 52, 1994).

[12] U. Naher, S. Björholm, S. Frauendorf, F. Garcia and C. Guet, *Physics Reports* 285, 245 (1997).

[13] J. Jellinek (ed.), *Theory of Atomic and Molecular Clusters. With a Guide to Experiments*, (Springer Series in Cluster Physics, Berlin, 1999).

[14] K.-H. Mewis-Broer (ed.), *Metal Clusters at Surfaces. Structure, Quantum Properties, Physical Chemistry*, (Springer Series in Cluster Physics, Berlin, 1999).

[15] J.M. Eisenberg, and W. Greiner, *Nuclear Theory. Vol. 1. Collective and Particle Models*, (North Holland, Amsterdam, 1985).

[16] A.G. Lyalin, S.K. Semenov, A.V. Solov'yov, N.A. Cherepkov and W. Greiner, *J. Phys. B* 33,

3653 (2000).

[17] A.G. Lyalin, S.K. Semenov, A.V. Solov'yov, N.A. Cherepkov, J.-P. Connerade, and W. Greiner, *J. Chin. Chem. Soc. (Taipei)* 48, 419 (2001).

[18] A.M. Atveentsev, A. Lyalin, IIA. Solov'yov, A.V. Solov'yov and W. Greiner, submitted to *Int. Journal of Modern Physics E* (2002); LANL preprint arXiv:physics/0207085 v2, 26 July 2002 (<http://arxiv.org>).

[19] L.G. Gerchikov, A.V. Solov'yov, W. Greiner, *International Journal of Modern Physics E* 8, 289 (1999).

[20] L.G. Gerchikov, A.N. Ipatov, A.V. Solov'yov and W. Greiner, *J. Phys. B: At. Mol. Opt. Phys.* 33, 4905 (2000).

[21] A.V. Solov'yov, in *Atomic Clusters and Nanoparticles* (Ref.[7]).

[22] IIA. Solov'yov, A.V. Solov'yov and W. Greiner, *Phys. Rev. A* 65, 053203 (2002).

[23] F. Reuse, S.N. Khanna, V. de Coulon and J. Buttet *Phys. Rev. B* 39, 12911 (1989).

[24] F. Reuse, S.N. Khanna, V. de Coulon and J. Buttet *Phys. Rev. B* 41, 11743 (1990).

[25] V. Kumar and R. Car *Phys. Rev. B* 44, 8243 (1991).

[26] P. Delaly, P. Ballone and J. Buttet *Phys. Rev. B* 45, 3838 (1992).

[27] J. Akola, K. Rytkonen and M. Manninen *Eur. Phys. J. D* 16, 21 (2001).

[28] Li. Serra, P.-G. Reinhard and E. Suraud *Eur. Phys. J. D* 18, 327 (2002).

[29] Th. Diedrich, T. Doppner, J. Braune, J. Tiggesbaumker and K.-H. Mewe-Broer, *Phys. Rev. Lett.* 86, 4807 (2001).

[30] T. Doppner, T. Diedrich, J. Tiggesbaumker and K.-H. Mewe-Broer, *Eur. Phys. J. D* 16, 13 (2001).

[31] M.J. Frisch et al, computer code GAUSSIAN 98, Rev. A. 9, Gaussian Inc., Pittsburgh, PA, 1998.

[32] James B. Foresman and Jeen Frisch *Exploring Chemistry with Electronic Structure Methods* (Pittsburgh, PA: Gaussian Inc, 1996)

[33] A.D. Becke, *Phys. Rev. A* 38, 3098 (1988).

[34] C. Lee, W. Yang and R.G. Parr, *Phys. Rev. B* 37, 785 (1988).

[35] R.G. Parr and W. Yang, *Density-Functional Theory of Atoms and Molecules*, Oxford University Press, Oxford, New York, 1989).

[36] J.P. Perdew, in *Electronic Structure of Solids '91*, edited by P. Ziesche and H. Eschrig

(Akademie Verlag, Berlin, 1991), p. 11.

[37] K. Burke, J.P. Perdew and Y. Wang, in *Electronic Density Functional Theory: Recent Progress and New Directions*, edited by J.F. Dobson, G. Vignale and M. P. Daus (Plenum, 1998).

[38] C.M. Ller and M. S. Plessset *Phys. Rev.* **46**, 618 (1934).

[39] K.P. Huber and G. Herzberg, *Molecular Spectra and Molecular Structure. IV. Constants of Diatomic Molecules*, (Van Nostrand Reinhold, New York, 1979)

[40] J.L. Martins, J. Buttet and R. Car, *Phys. Rev. B* **31**, 1804 (1985)

[41] V. Bonacic-Koutecky, P. Fantucci, J. Koutecky, *Phys. Rev. B* **37**, 4369 (1988)

[42] N.W. Ashcroft and N.D. Mermin, *Solid State Physics*, (Saunders College Publishing, New York, 1976)

[43] C. Kittel, *Introduction to Solid State Physics*, 7th edn., (John Wiley and Sons, New York, 1996)

[44] S.M. Reimann, M. Koskinen, H. Hakkinen, P.E. Lindelof and M. Manninen, *Phys. Rev. B* **56**, 12147 (1997).

[45] J.P. Perdew and A. Zunger, *Phys. Rev. B* **23**, 5048 (1981).

[46] D.M. Ceperley and B.J. Alder, *Phys. Rev. Lett.* **45**, 566 (1980).

[47] J.P. Perdew *Phys. Rev. B* **33**, 8822 (1986).

[48] R. Car and M. Parrinello, *Phys. Rev. Lett.* **55**, 2471 (1985).

[49] J.P. Perdew, K. Burke and M. Ernzerhof, *Phys. Rev. Lett.* **77**, 3865 (1996); *ibid.*, **78**, 1396 (E) (1997).